Use of the 3D Radon transform to examine the properties of oceanic Rossby waves

Peter G Challenor, Paolo Cipollini and David Cromwell

James Rennell Division for Ocean Circulation and Climate,

Southampton Oceanography Centre, Southampton SO14 3ZH, U.K.

29 November 2000

Revised version

Journal of Atmospheric and Oceanic Technology

Corresponding author address: David Cromwell, James Rennell Division for Ocean Circulation and Climate, Southampton Oceanography Centre, European Way, Southampton SO14 3ZH, U.K. E-mail: ddc@soc.soton.ac.uk

ABSTRACT

One of the most successful applications of satellite-borne radar altimeter data over the oceans in recent years has been the extraction of information about long-wavelength baroclinic Rossby (or planetary) waves, which play a significant role in ocean circulation and climate dynamics. These waves cross ocean basins from east to west at speeds of few centimetres per second at mid-latitudes. The cross-basin propagation time may therefore be several months or even years and an accurate estimation of the speed of the waves is important. We review the methods for obtaining information on Rossby wave velocity from altimetry data, particularly the two-dimensional Radon transform. Unfortunately the use of longitude-time plots, although it allows the estimation of the zonal phase speeds, does not give any information on the speed vector when the propagation of the waves is not purely zonal (east-west). We show how the two-dimensional Radon Transform can be generalised to three dimensions, enabling not only the true propagation velocity component to be determined, but also the direction of the waves and thus any deviation from the pure-westward case. As examples of the application of this extended technique, we show maps of direction, speed and energy of Rossby waves in the North Atlantic Ocean.

1. INTRODUCTION

Because of its repeat sampling and global quasi-synoptic capability, the satellite-borne radar altimeter is an excellent instrument for looking at large-scale oceanographic phenomena with surface signatures which may be difficult to detect in conventional oceanographic measurements such as current meter moorings and hydrographic sections. One such dynamical phenomenon is long-wavelength baroclinic Rossby waves. These waves, which are a special type of planetary wave (whose existence is due to earth rotation), play a fundamental role in atmospheric and ocean dynamics. Their name derives from the work of Rossby (1939), who built on the theory of planetary waves first formulated by Hough (1897).

Oceanic Rossby waves are important for a number of reasons: they maintain the strong western boundary currents such as the Kuroshio and the Gulf Stream; they are the main oceanic response to changes in atmospheric forcing; and they are the only means (other than boundary waves) by which information is transferred from the eastern ocean boundaries to the west (e.g. Gill, 1982). The speed of Rossby wave propagation is important in determining the oceanic response time to disturbances from the equilibrium state. Rossby waves can even be responsible for disturbing the position of the western boundary currents. By using a general ocean circulation model and data from the space-borne Geosat altimeter, Jacobs et al. (1994) present evidence for the existence an extra-tropical Rossby wave in the North Pacific, generated by the El Niño event of 1982-83. This wave has also been observed by Jacobson and Spiesberger (1998) in expendable bathythermometric (XBT) data. Jacobs et al. (1994) suggest that after a decade's delay this wave induced a shifting of the Kuroshio Current in the north-west Pacific which may have affected the climate of North America, and which may have been responsible for the dramatic meteorological events in North America in 1993, such as the Mississippi flooding (McPhaden, 1994). In short, as well as being one of the ways the ocean itself responds to climate events, Rossby waves may also be a generator of climate change and weather variability.

The first detection of Rossby waves in altimetry was achieved with Geosat data (e.g. Le Traon and Minster, 1993; Tokmakian and Challenor, 1993). However, tidal aliasing arising from the Geosat sampling pattern meant that any error in the M2 tidal component aliased to a signal with properties

similar to the first baroclinic mode Rossby wave (Parke *et al.,* 1998). ERS and TOPEX/POSEIDON (hereafter T/P) are largely free of this problem and the Rossby wave signal can be clearly seen. Chelton and Schlax (1996) showed that the speed of the Rossby waves as detected by T/P is faster than that predicted from linear theory using data atlases of ocean climatology . This observation has prompted a number of theoretical papers which have attempted to explain this discrepancy (Killworth et al, 1997; Qiu et al., 1997; Dewar, 1998; White et al., 1998; Killworth and Blundell, 1999).

All of these papers, bar one, have been concerned with the zonal (east-west) speed of Rossby waves. (The exception is Dewar, 1998, who produced characteristics of long baroclinic Rossby waves not restricted to constant latitude lines). In practice, however, Rossby waves do not always propagate solely westwards: their speed may have a North-South component as well. It is expected that this will be particularly important when they interact with topography, over mid-ocean ridges for example (Killworth and Blundell, 1999). In this paper we review the methods of extracting velocities as seen through zonal sections, in particular the 2D Radon transform, and present a method which handles real 3D datasets as functions of (longitude, latitude, time) in order to cope with non-zonally propagating signals. We conclude by giving an example from the North Atlantic Ocean.

2. TWO-DIMENSIONAL ANALYSES

The basis for the detection of Rossby waves in altimeter measurements of sea surface height (SSH) anomaly is the Hovmöller diagram or longitude/time plot. (The SSH anomalies are normally calculated with respect to a multi-year mean SSH). To construct such a diagram, altimeter data are interpolated to a grid and zonal sections are ‘stacked’ to give a two-dimensional plot whose x-axis is longitude and y-axis is time. Westward propagating signals can clearly be seen in such diagrams (not shown) as areas of local maxima and minima moving linearly from right to left across the diagram. The speed of these signals can easily be calculated by hand by simply taking the slope of the diagonal alignments of maxima and minima. Whilst such a procedure is easy to carry out on a

few diagrams, a more automated and objective method is required to calculate propagation speeds for entire ocean basins.

A number of two-dimensional data processing techniques can be applied to the longitude/time diagrams in order to study the properties of zonally propagating signals. For example, the two-dimensional Fourier transform yields the different spectral components of longitude/time plots which appear as peaks in the frequency-wavenumber domain, and has been used for a number of years for the detection of Rossby waves (e.g. Le Traon and Minster, 1993, Tokmakian and Challenor, 1993). One advantage of this technique is that it allows the detection of single components of the propagating signals, which may correspond to different baroclinic modes as suggested by Cipollini et al. (1997). Distinct baroclinic modes of propagation are also observed by Subrahmanyam et al. (2000), who applied the same technique to longitude-time plots of TOPEX/POSEIDON (T/P) SSH anomalies in the tropical Indian Ocean.

An alternative method is to mathematically define the technique used to measure speed by hand. Such a signal processing method is the Radon transform, first described by Radon (1917).

2.1 Definition of the Radon Transform

Let $f(\mathbf{x})$ be a function of the 2-D vector $\mathbf{x}=(x,y)$ (in our case $f(\mathbf{x})$ is the wavefield in the longitude/time plot and x, y are longitude and time, respectively). If L is an arbitrary line at an angle θ with respect to the x axis, the Radon transform (Deans, 1983) is defined as the projection of $f(\mathbf{x})$ on L, that is

$$p(s,\theta) = \int_u f(\mathbf{x})du \qquad (1)$$

where u is the direction orthogonal to L (along which the integral summation is performed) and s is the coordinate on L. Note that, for a given θ, the Radon transform is a 1-D function of the line coordinate s. We can rewrite (1) in terms of coordinates x and y, as shown in Figure 1:

$$p(x',\theta) = \int_{y'} f(x,y)\Big|_{\substack{x=x'\cos\theta - y'\sin\theta \\ y=x'\sin\theta + y'\cos\theta}} dy' \qquad (2)$$

The Radon transform has many varied applications: for example, in medical imaging; the processing of seismic data to find subsurface rock interfaces; and the detection of ship wakes in satellite images. In satellite remote sensing of the oceans, Chelton and Schlax (1996) applied the Radon transform in their global analysis of Rossby waves observed in T/P data, as did Polito and Cornillion (1997) in their intensive study of Rossby waves in the North Atlantic; Cipollini et al. (1997, 1999) applied it to T/P data in the North Atlantic finding strong Rossby wave propagation near the Azores Current; while Hill *et al.* (2000) used the method to detect Rossby waves in global sea surface temperature data from the Along-Track Scanning Radiometer on board ERS-1.

In all these applications, the essential method is to transform two-dimensional images with lines into a domain of possible line parameters (e.g. slope, which equates to speed in a longitude/time plot), whereby each line in the image will yield a peak at the corresponding line parameter in the transform domain. When the focus of the analysis is on the propagation speed, rather than on the wavelength and period characteristics of the single components, the Radon transform (RT) is more appropriate than the Fourier transform (FT).

As with any transform, the selection of the longitude/time subdomain on which it is applied requires a trade-off between resolution and homogeneity. In the FT case the longitude/time space is transformed into a wavenumber-frequency space so any periodic signal with a constant wavelength and period will correspond to a distinct peak in that space. If the selected subdomain is too narrow, adjacent peaks will be indistinguishable from each other. On the other hand, if the interval is too large, so that the propagation characteristics vary significantly, or if the waves are not periodic in the first place, the interpretation of the transform becomes difficult. A consequence of this is that the FT is not suited for the study of single waves, such as the soliton observed by Jacobs et al. (1994) in the Pacific as a result of the 1982-83 El Niño.

As with the FT, the RT needs homogeneity to show distinct, well-identifiable peaks; only, in this case, it is the speed of the waves (regardless of their periodicity) that has to be reasonably constant within the selected subdomain. This implies that the RT can cope with solitons or other non-periodic phenomena provided they propagate at constant or quasi-constant speed in the selected subset of the data. It is also possible to generalise the RT as projection along curves, in order to

extract information on signals propagating with a variable speed rather than with a constant one, although we will not pursue this further here.

2.2 Application of the 2D Radon Transform to altimeter data

The RT as used in this study consists of two parts. First, the Hovmöller diagram is projected onto a line at a range of angles from 0° (the *x* or longitude axis) to 180° (the *y* or time axis is at 90°). When the line is perpendicular to the alignment of crests and troughs of the Rossby waves the projection will have maximum energy (i.e. maximum variance). Thus, to find the direction of travel of the waves in the space-time diagram (which is of course their speed) we determine the projection which gives maximum variance and note the elevation angle, θ, of the perpendicular to that projection.

Mathematically, this is expressed by finding the value θ, for which $\int p^2(x',\theta)dx'$, with p from equation (2) is a maximum, i.e. forming the projected sum of data from the (*x,y)* plane to the *x'* axis, where the transformation of coordinates is defined by: $x=x'\cos\theta-y'\sin\theta;\ y=x'\sin\theta+y'\cos\theta$, as depicted in Figure 1, and computing its energy. (In a discretized case this energy is $\sum_i p^2(x_i')$, where x_i' are the bins on the x' axis).

It is worth noting that the FT and RT are related by means of the *Projection-Slice theorem*: the RT at a given θ corresponds to the inverse FT of a slice taken at the same angle θ in the Fourier space. This is important as the lines at an angle θ, both in the longitude-time space and in the wavenumber-frequency space, are lines of constant speed, which can be readily computed from θ. This implies that computing the RT of the longitude-time plot for different values of θ, and then its energy, is equivalent to computing the energy in the spectrum along lines of constant speed, and it is the most straightforward method to find the value of the speed for which that energy is maximum. Rossby wave speeds in the zonal direction are thus relatively easy to calculate using the Radon transform.

3. THE THREE-DIMENSIONAL RADON TRANSFORM

When the propagation of Rossby waves is not purely westward, zonal sections as used in longitude/time plots still give the zonal phase speed $v_Z = \omega/(2\pi k_x)$, where $\omega = 2\pi f$ is the angular frequency and k_x the zonal wavenumber (this speed can be readily compared with the zonal phase speed estimated from the linear theory), but no information on the true speed vector of the waves. Figure 2 depicts a wave crest travelling at a direction φ relative to pure westward, at two subsequent instants t and $t + \Delta t$. In the time Δt the crest travels a space vector $\Delta\mathbf{s}_{TRUE}$, so the speed vector is $\mathbf{v}_{TRUE} = \Delta\mathbf{s}_{TRUE} / \Delta t$. The space travelled by the crest as seen through a zonal section is $\Delta s_Z = |\Delta\mathbf{s}_{TRUE}|/\cos\varphi \geq |\Delta\mathbf{s}_{TRUE}|$, and the corresponding zonal speed is $v_Z = \Delta s_Z / \Delta t = |\mathbf{v}_{TRUE}|/\cos\varphi \geq |\mathbf{v}_{TRUE}|$. It is important that we remove the inherent limitation of longitude/time plots because, as mentioned above, Rossby wave speed (not only the zonal phase speed, but also the magnitude of the speed vector) is an important parameter related to the response time of the oceans to forcing. Moreover, possible deviations of the direction from the pure westward propagation predicted by simple theory have been suggested by recent theoretical work such as Killworth and Blundell (1999), who studied the effects of varying bottom topography on Rossby wave propagation. Observations of the deviation of speed from the pure-westward case are thus needed. To study the directional properties of Rossby waves and estimate the magnitude of their speed vector we need to look at cuboids of data, not just longitude-time slices. Consequently, we have to use three-dimensional techniques such as the 3D-FT and the 3D-RT. In the present paper we deal with the latter, which, as we showed in the 2D case above, is more appropriate for evaluating the magnitude and direction of velocities.

The 3D Radon Transform is defined in the same way as in equation (1), except that **x** is now a vector in 3D and the integral is a projection on a plane, whose orientation is identified by a pair of angles (θ,φ), rather than on a line (see figure 3):

$$p(x', y', \theta, \varphi) = \int_{z'} f(x, y, z)\, dz' \qquad (3)$$

The formal details are in Deans (1983). The transformation of coordinates is expressed by:

$$\begin{aligned} x' &= x\cos\varphi\cos\theta + y\sin\varphi\cos\theta + z\sin\theta \\ y' &= -x\sin\varphi + y\cos\varphi \\ z' &= -x\cos\varphi\sin\theta - y\sin\varphi\sin\theta + z\cos\theta \end{aligned} \qquad (4)$$

The above equations can be easily obtained by considering the transformation of coordinates as the result of two consecutive rotations, the first one of an *azimuth* φ around the z axis and the second one of an *elevation* θ around the y' axis, as shown in figure 3.

When applying this concept to our dataset of gridded satellite data, rather than generate two-dimensional plots with longitude and time axes, we will now work with a cube of data, retaining the latitude dimension. Our objective is to find linear alignments of crests and troughs within the cube – the signature of possible Rossby waves. This can be done in our 3D space by projecting the data onto a $(x'y')$-plane oriented at (θ,φ) and summing the projected data into 2D bins (see Figure 3). Doing so we have a discretisation of the 3D Radon transform. We then look for the pair of values $\theta_{max},\varphi_{max}$ which maximise the energy of the projected sum. These identify the plane orthogonal to the main direction of the alignments, i.e. the main direction z' of propagation of crests and troughs in the cuboid. Elevation θ can then be converted into speed as for the 2D case, while azimuth φ yields the geographical direction of propagation.

In practice, as seen for the 2D transform, a trade-off has to be made between the assumption of homogeneity and spatial resolution. So the 3D analysis is carried out, not on the complete cuboid of data, but on successive 'sub-domains' defined by a sliding window in latitude-longitude space, e.g. 5° x 11°. Hence, the Rossby wave propagation characteristics that are determined are the averaged properties in a spatial window of this size. In the present paper, we include the complete time series in each spatial window. In principle, however, one could choose to apply the 3D Radon transform to subsets of the complete time interval spanned by the data, and thereby investigate temporal changes in Rossby wave propagation characteristics, although it must be recalled that shortening the time interval also lowers the resolution. A detailed study of the resolution of the Radon Transform will be the object of a subsequent study.

4. APPLICATION OF THE 3D RADON TRANSFORM

4.1 Processing of TOPEX/POSEIDON (T/P) data

The T/P satellite, launched in August 1992, carries two altimeters ('TOPEX' and 'POSEIDON') (see Fu et al., 1994, for details). However, because they have been carefully intercalibrated we may treat them as one altimetric dataset. The satellite lays down a ground track of passes 2.7^o apart in longitude, repeated every 9.92 days. We applied a standard set of corrections for orbit errors, atmospheric delays, tides and sea state effects (see Cipollini et al, 1997). A mean height profile is calculated for the three calendar years 1993-1995, and SSH anomalies are computed relative to that. The accuracy of the SSH retrieval with T/P is of the order of 2 cm, as found by Cheney et al. (1994) by comparison with tide gauges. Each cycle of data is then interpolated onto a 1^o by 1^o grid. The interpolation, which uses a Gaussian weighted mean of all the data within 200km of a grid point, reduces the instrument and correction errors whilst leaving the larger scale signal relatively unaffected. Chelton and Schlax (1996) suggest that signals with an amplitude of ~1 cm may be observable. 234 10-day T/P cycles were used, spanning October 1992 – February 1999.

4.2 3D RT of T/P data in the North Atlantic

We used the discretised form of the 3D Radon transform described above and applied to the processed, gridded T/P data volume in the North Atlantic. Tests were undertaken with a variety of spatial windows; 5° (lat) x 5° (lon), 5° (lat) x 9° (lon), 9° (lat) x 9° (lon) and 5° (lat) x 11° (lon). This last choice of 5° (lat) x 11° (lon) was found to be a reasonable compromise between smoothing of signal properties and noise reduction to enable propagating signal detection. Limiting the latitude range to 5° is a reasonable choice (e.g. Polito and Cornillion, 1997) to suppress excessive smoothing of the latitudinally-dependent Rossby wave speed. Note that a Fourier analysis method would require 2 – or better, 3 - samples per wavelength to satisfy the Nyquist criterion, and that a window length of 11° in longitude would be insufficient to resolve the Rossby waves in low latitudes where wavelengths can reach 2000 km or more. The Radon Transform suffers a similar limitation at low latitudes. A way to overcome this limitation would be the use of different spatial windows (with longer longitude spans closer to the equator, which obviously means to reduce the

resolution in the location of the waves) but here for the sake of simplicity we restrict our analysis to a single window.

The analysis presented here was therefore applied to a 5° (lat) x 11° (lon) x 234 (cycle) sub-domain, which in turn was stepped across the whole dataset in 2°x2° intervals. Figure 4 shows a polar plot of the Radon transform energy centred at 34°N, 36°W, revealing strong quasi-westward propagation of energy, with a maximum at a deviation of 10° to the south relative to a pure westward propagation. The speed corresponding to the maximum energy is ~2.6 cm/s, consistent with the results of Cipollini et al. (1997) who found exactly the same value from a 2D analysis of T/P data over the 38°W to 8°W longitude span at 34°N.

The 3D Radon Transform over the whole basin was performed using a complete azimuth range of 0° to 360°, in increments of 5°. The elevation range in the 3D RT calculation was 0° to 80°, in steps of 1°. This comfortably covers the range of possible Rossby waves speeds over the latitude range presented below (16°N – 54°N).

After the 3D Radon Transform energy was calculated for the North Atlantic basin, we applied various screening of the results in azimuth, speed and energy to highlight propagating Rossby waves. We selected only those speeds within an interval in velocity space, thus suppressing too-fast and too-slow propagating signals, including the stationary and near-stationary ones related to seasonal heating and cooling. This screening was based on *a priori* knowledge of propagating baroclinic Rossby waves: namely, the known latitudinal dependence of propagation speed. Chelton and Schlax (1996) demonstrated that observed zonal Rossby wave speeds exceed predicted speeds from the linear theory, often by a factor 2 or more, particularly at mid-latitudes. We then selected only those energy maxima whose speed was within 0.5 and 3 times the expected (linear-theory) first-mode baroclinic Rossby wave speed at that latitude. We believe that this interval includes the vast majority of signals that are genuine Rossby waves. To highlight westward or quasi-westward propagating waves, the velocity screening was combined with screening of results in terms of azimuth. Again, a conservative approach was adopted, choosing $230^o < \varphi < 310^o$, that is only those signals with a propagation direction within ± 40° from pure westward. A further screening was done on the energy of the observed maxima, retaining only those above a threshold. The threshold was

selected after MonteCarlo trials with fields of pure gaussian noise with a RMS value of 2cm, and ensures that the peaks observed are significant above the 95% confidence level. Different types of screening may be required for different datasets, e.g. sea surface temperature, which we do not consider in this paper but clearly shows the signature of Rossby waves (Hill et al., 2000).

The results are presented in figure 5. Empty 2^ox2^o grid cells correspond to locations where no maxima in the 3D RT passed the screening described above. Visual cross-checking with polar plots of the type shown in Figure 4 confirmed that there were no distinct westward or quasi-westward propagating signals at such locations. Figure 5a shows the direction of the resulting signals. As can be seen from the figure, most energy at mid-latitudes actually propagates within 10^o of due west. Figure 5b shows the speed of the waves corresponding to the signals selected in Figure 5a. The energy of these waves (in arbitrary units) is shown in Figure 5c. It is worth noting that the results are robust in that they are in agreement with westward-propagating features observed in Hovmöller plots at a number of selected locations (not shown here). Figure 6 shows a comparison between zonal averages of speeds over the North Atlantic basin, including the zonal speed derived from our results (figure 5b divided by the cosine of the deviation in figure 5a), the zonal phase speed predicted from the linear theory, and the zonal phase speed predicted from the extended theory by Killworth et al. (1997). The same figure includes also the three propagation speeds from T/P data measured in the extra-tropical North Atlantic by Chelton and Schlax (1996).

5. DISCUSSION

In the plot of the direction of propagation of the waves (Figure 5a), we observe a wide mid-latitude zonal band (approximately 20°N to 40°N) where the 3D method retrieves a quasi-westward signal (within ±10° from pure westward). In this band, the topography has no clear effect, possibly because the longitudinal extent (11^o) of the 3D Radon transform window is greater than the lengthscale of potentially important topographic features, e.g. the width of the mid-Atlantic ridge.

The propagation speed of the waves (Figure 5b) increases equatorwards in accordance with the theory. We also note at mid-latitudes (around 34-36°N) a distinct increase in speed as the waves move to the western part of the basin, consistent with previous results (Chelton and Schlax, 1996; Cipollini et al., 1996). There are no clear effects of topography on speed, again because they are

probably averaged out within the 3D RT window. It is known, however, that topography can have important local effects on Rossby wave velocity (e.g. Killworth and Blundell, 1999).

From Figure 5c we note high energy in the region of the Gulf Stream. While this region is obviously very energetic at a number of different scales, it has to be stressed that the energy plotted here is only that associated with the westward propagating signals passing the screening described in the previous section, so it is most likely to be associated with Rossby waves. We also observe that in the eastern North Atlantic there is a zonal band of enhanced Rossby wave energy centred on 34°N. This zonal waveguide of stronger Rossby wave propagation just south of the Azores Current is consistent with previous T/P observations analysed using standard Fourier and 2D Radon transform methods (Cipollini et al. 1996, 1997, 1999). The theoretical results by Killworth and Blundell (1999) show a similar waveguide in the North Atlantic, with focussing of planetary wave energy around 36°N.

The most likely explanation for the scatter in the deviation north of 40°-45°N is that Rossby waves become evanescent and do not propagate at all beyond this critical latitude [see eqn. 12.3.16 in Gill, 1982]. Moreover, as the propagation speed decreases, the effects of the mean barotropic flow on the speed and direction of the waves become more evident; in other words, some of the scatter might be due to noticeable advection of very slow-moving disturbances by the mean barotropic flow at the depth of the thermocline.

The observed results for the basin-wide averages of zonal speed at different latitudes, plotted in figure 6, show that the waves tend to go significantly faster than predicted by the linear theory at latitudes between 27° and 45°. In the same latitudinal band the results are in broad agreement with the zonal mean for the North Atlantic from the extended theory by Killworth et al. (1997), although the latter shows greater variability with latitude (the meridional variability in our analysis is obviously smoothed by the use of a 5 degree window in latitude as discussed in section 4.2.). The speeds measured by Chelton and Schlax (1996) at 29.73° and 32.37° are significantly greater than both our results and those by Killworth et al.; however, the three speeds (Chelton and Schlax's, Killworth et al's and this study) almost coincide (at ~1.5 times the speed expected from the linear theory) in the most energetic waveguide around 34°N.

At latitudes equatorward of 25°N the 3D RT method picks up waves slower than the theory (except at 16°N where it detects a fast signal close to the western boundary). Interestingly, also Killworth et al.'s (1997) phase speeds are lower than the linear theory predictions in the latitudinal band 20-22°N. However our estimates are still approximately 15-20% lower than Killworth et al.'s in the 20°-24°N interval. One possible explanation of this discrepancy could be that at those latitudes the transform is highlighting higher-order, slower baroclinic modes of propagation, but the behaviour of the 3D RT at low latitudes and any issues related to its resolution will obviously have to be investigated further.

Before going into too much detail on the particular oceanographic results, it has to be recalled that the main purpose of this paper was to describe the 3D-RT methodology used and to show (with the North Atlantic example) that it allows a study of the directional properties of propagating features like baroclinic Rossby waves. We believe that this has now been established. We are now planning to apply the 3D Radon transform analysis to the global ocean and to study quantitatively the correlation between wave properties and topography. We hope that such observational results will continue to stimulate the development of theoretical analyses of Rossby wave propagation.

6. ACKNOWLEDGMENTS

We thank NASA and AVISO for the provision of TOPEX/POSEIDON altimeter data, and Jeff Blundell, Katy Hill, Peter Killworth, Graham Quartly, Ian Robinson, and Stefano Raffaglio for their kind help and suggestions. We are grateful to Helen Snaith for support of the altimeter processing software.

REFERENCES

Chelton, D. B. and M. G. Schlax, Global observations of oceanic Rossby waves, *Science*, *272*, 234-238,1996.

Cheney, R., L. Miller, R. Agreen, N. Doyle and J. Lillibridge, TOPEX/POSEIDON: the 2-cm solution, *Journal of Geophysical Research*, *99*, 24555-24563, 1994.

Cipollini, P., D. Cromwell, and G. D. Quartly, Variability of Rossby wave propagation in the North Atlantic from TOPEX/POSEIDON altimetry, *Proceedings of IEEE International Geoscience and Remote Sensing Symposium (IGARSS '96)*, Lincoln (Nebraska), 27-31 May 1996, Piscataway: IEEE, vol. I, pp. 91-93, 1996.

Cipollini, P., D. Cromwell, M. S. Jones, G. D. Quartly and P. G. Challenor, Concurrent TOPEX/POSEIDON altimeter and Along-Track Scanning Radiometer observations of Rossby wave propagation near 34ºN in the Northeast Atlantic, *Geophys. Res. Letters*, *24*, 889-892, 1997.

Cipollini, P., D. Cromwell and G. D. Quartly, Observations of Rossby Wave propagation in the Northeast Atlantic with TOPEX/POSEIDON altimetry, *Adv. Space Res.*, *22*, 1553-1556, 1999.

Deans, S.R., The Radon transform and some of its applications, John Wiley and Sons, New York, 1983.

Dewar, W., On too-fast baroclinic planetary waves in the general circulation, *J. Phys. Oceanogr.*, 28, 1739-1758, 1998.

Fu, L.-L., E.J. Christensen, C.A. Yamarone Jr, M. Lefebvre, Y. Menard, M. Dorrer, and P. Escudier, TOPEX/POSEIDON mission overview, *Journal of Geophysical Research*, *99*, 24369-24381, 1994.

Gill, A. E., *Atmosphere-Ocean Dynamics*, Academic Press, San Diego, 1982.

Hill, K., I. S. Robinson, and P. Cipollini, Propagation characteristics of extratropical planetary waves observed in the ATSR global sea surface temperature record, *Journal of Geophysical Research, 105(C9)*, 21927-21945, 2000.

Hough, S. On the application of harmonic analysis to the dynamical theory of the tides, Part I. On Laplace's 'oscillations of the first species', and on the dynamics of ocean currents. *Philos. Trans. Roy. Soc., A,* **189,** 201-257, 1897.

Jacobs, G. A., H. E. Hurlburt, J. C. Kindle, E. J. Metzger, J. L. Mitchell, W. J. Teague, and A. J. Wallcraft, Decade-scale trans-Pacific propagation and warming effects of an El Nino anomaly, *Nature, 370*, 360-363, 1994.

Jacobson, A. R. and J. L. Spiesberger, Observations of El Niño-Southern Oscillation induced Rossby waves in the northeast Pacific using in situ data, *J. Geophys. Res.*, 103, 24585-24596, 1998.

Killworth, P. D., D. B. Chelton and R. deSzoeke, The speed of observed and theoretical long extra-tropical planetary waves, *J. Phys. Oceanogr., 27,* 1946-1966, 1997.

Killworth, P. D. and J. R. Blundell, The effect of bottom topography on the speed of long extra-tropical planetary waves. *J. Phys. Oceanogr., 29(10),* 2689-2710, 1999.

Le Traon, P.-Y. and J.-F. Minster, Sea Level Variability and Semiannual Rossby Waves in the South Atlantic Subtropical Gyre, *J. Geophys. Res., 98,* 12,315-12,326, 1993.

Levitus, S., Climatological Atlas of the World Ocean, *NOAA, Rockville, MD, Professional Paper 13, 173pp,* 1982.

McPhaden, M.J, The eleven-year El Niño?, *Nature,* **370**, 326, 1994.

Parke, M. E., G. Born, R. Leben, C. McLaughlin, and C. Tierney, Altimeter sampling characteristics using a single satellite, *J. Geophys. Res., 103*, 10,513-10.526, 1998.

Polito, P. S., and P. Cornillon, Long baroclinic Rossby waves detected by TOPEX/POSEIDON, *J. Geophys. Res., 102,* 3215-3235, 1997.

Qiu, B., W. Miao, and P. Müller, Propagation and delay of forced and free baroclinic Rossby waves in off-equatorial oceans, *Journal of Physical Oceanography*, *27* , 2405-2417, 1997.

Radon, J., Über die Bestimmung von Funktionen durch ihre Integralwerte längs gewisser Mannigfaltigkeiten, *Berichte Sächsische Akademie der Wissenschaften. Leipzig, Math.–Phys. Kl.*, *69*, 262-267, 1917. English translation in S.R. Deans, *The Radon transform and some of its applications*: John Wiley, pp. 204-217, 1983.

Rossby, C. Planetary flow patterns in the atmosphere. *Quart. Journ. Roy. Met. Soc.*, **66** (suppl.), 68-97, 1939.

Subrahmanyam, B., I. S. Robinson, J. R. Blundell and P. G. Challenor, Rossby waves in the Indian Ocean from TOPEX/POSEIDON altimeter and model simulations, *Int. J. Remote Sensing*, in press, 2000.

Tokmakian, R. T. and P. G. Challenor, Observations in the Canary Basin and the Azores Frontal Region Using Geosat Data, *J. Geophys. Res.*, *98*, 4761-477, 1993.

FIGURE CAPTIONS

Figure 1. Schematic of the two-dimensional Radon transform of a longitude-time section (see text for details).

Figure 2. Example of non-purely zonal wave propagation. The zonal phase speed is $v_Z = \frac{\Delta s_Z}{\Delta t} = \frac{1}{\Delta t}\frac{|\Delta \mathbf{s}_{TRUE}|}{\cos\varphi}$.

Figure 3. Three-dimensional Radon transform of gridded data volume (see text for details).

Figure 4. Polar plot of energy from the 5°(lat) x 11° (lon) x 234 cycles three-dimensional Radon Transform of T/P SSH anomalies centred at 34°N, 36°W. Due north is at the top of the polar plot, and so the 'compass angle' or azimuth φ yields the direction of wave propagation. Radial distance from the centre is the elevation angle θ, whose corresponding speed in cm/s is shown by the concentric lines. A strong energy peak can be seen at a speed of 2.6 cm/s and φ=260° (clockwise from N) corresponding to a deviation of 10° southward from pure westward propagation.

Figure 5. Deviation from pure westward propagation (a), speed magnitude $|\mathbf{v}_{TRUE}|$ (b) and energy (c) of the strongest energy maximum in a 3D Radon transform analysis of gridded TOPEX/POSEIDON data. The signal at each location has been selected after the screening described in section 4, that is from those propagating within ±40° of pure west (i.e. within the azimuthal range $230^\circ \le \varphi \le 310^\circ$) with speeds between 0.5 and 3 times the speed predicted at each latitude by the linear theory, and energy above a confidence threshold. The isobaths are for depths of 2000m (plotted in red) and 3500m (plotted in blue).

Figure 6. Comparison between basin-wide zonal averages of: i - the zonal phase speed predicted for the North Atlantic by the linear theory; ii - the zonal speed derived from this study (figure 5b divided by the cosine of the deviation in figure 5a); iii - the zonal phase speed predicted for the North Atlantic by the revised theory of Killworth et al. (1997). The figure also includes the three speeds measured by Chelton and Schlax (1996) from T/P data.

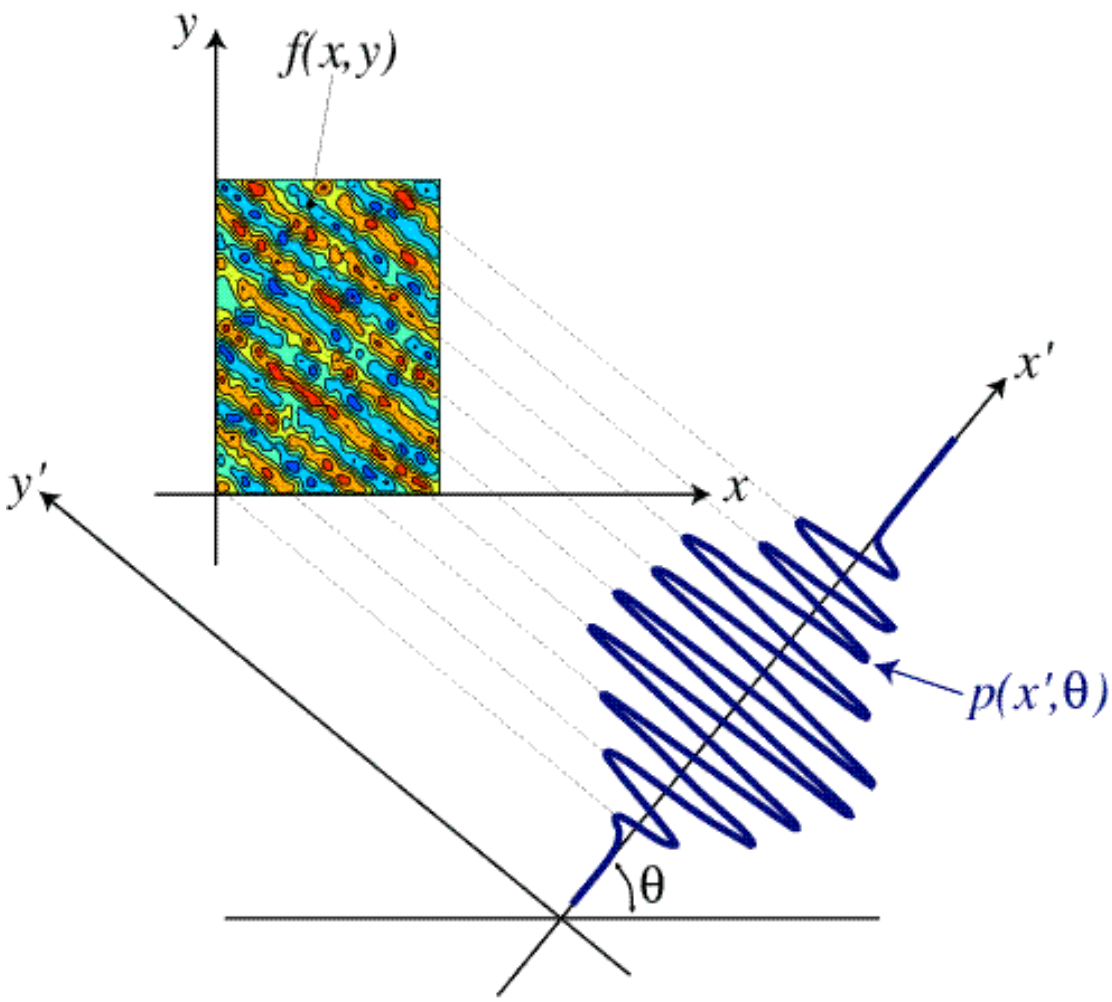

$$p(x',\theta) = \int_{y'} f(x,y) \Big|_{\substack{x = x'\cos\theta - y'\sin\theta \\ y = x'\sin\theta + y'\cos\theta}} dy'$$

Figure 1.

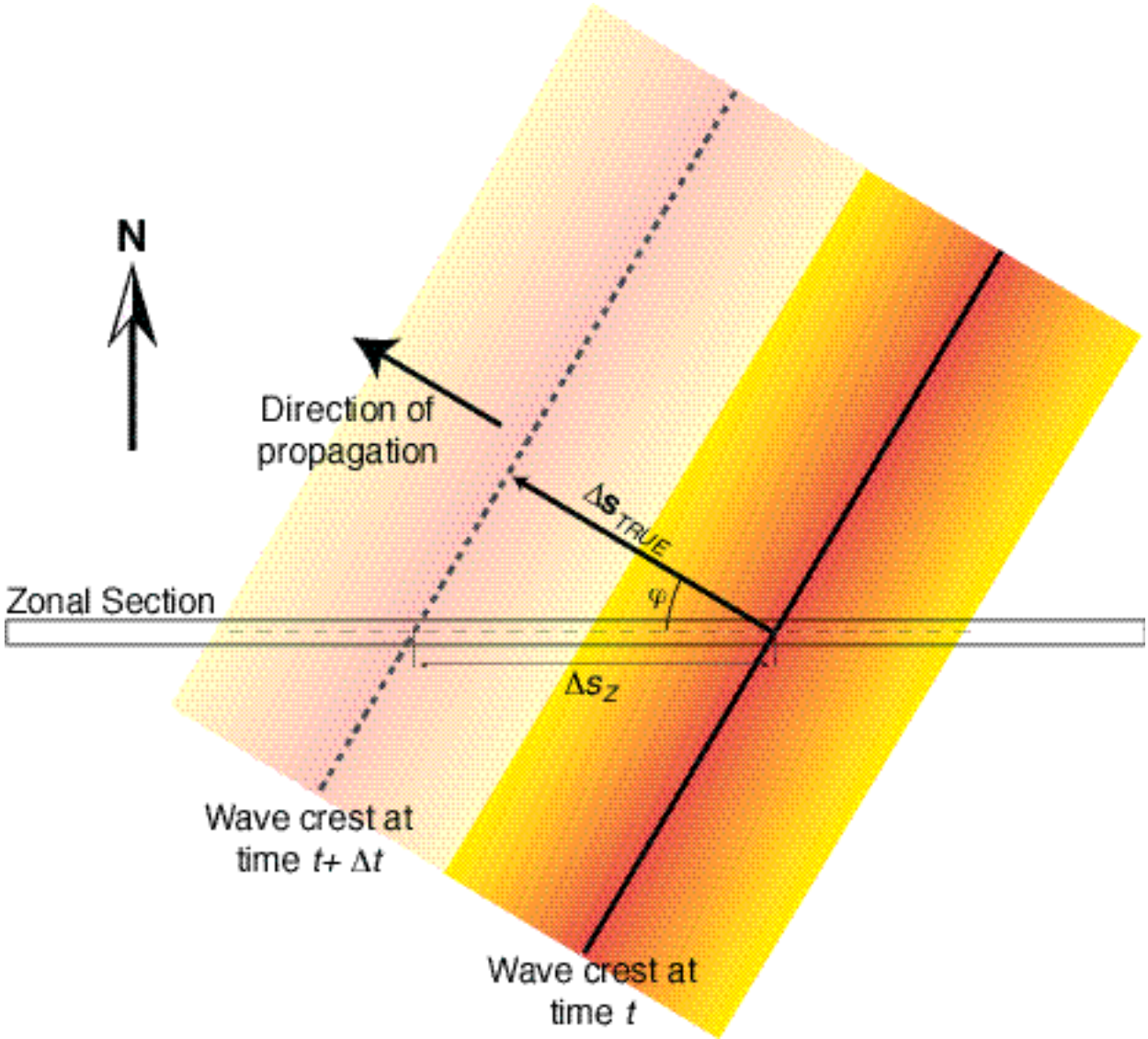
N
Direction of propagation
Δs_{TRUE}
φ
Zonal Section
Δs_z
Wave crest at time $t+\Delta t$
Wave crest at time t

Figure 2.

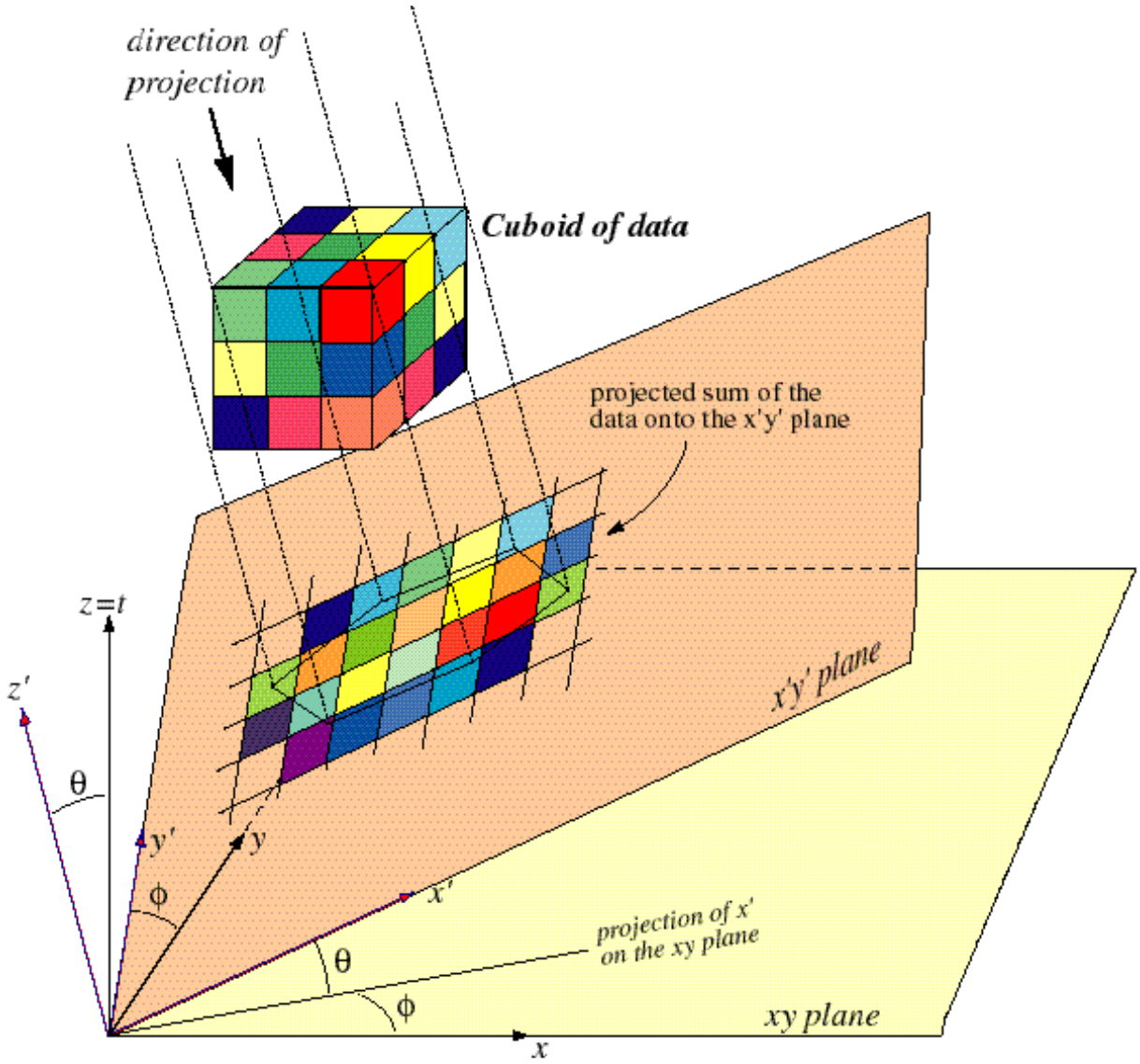
direction of projection
Cuboid of data
projected sum of the data onto the x'y' plane
z=t
z'
θ
y'
y
x'
ϕ
x'y' plane
projection of x' on the xy plane
θ
ϕ
xy plane
x

Figure 3.

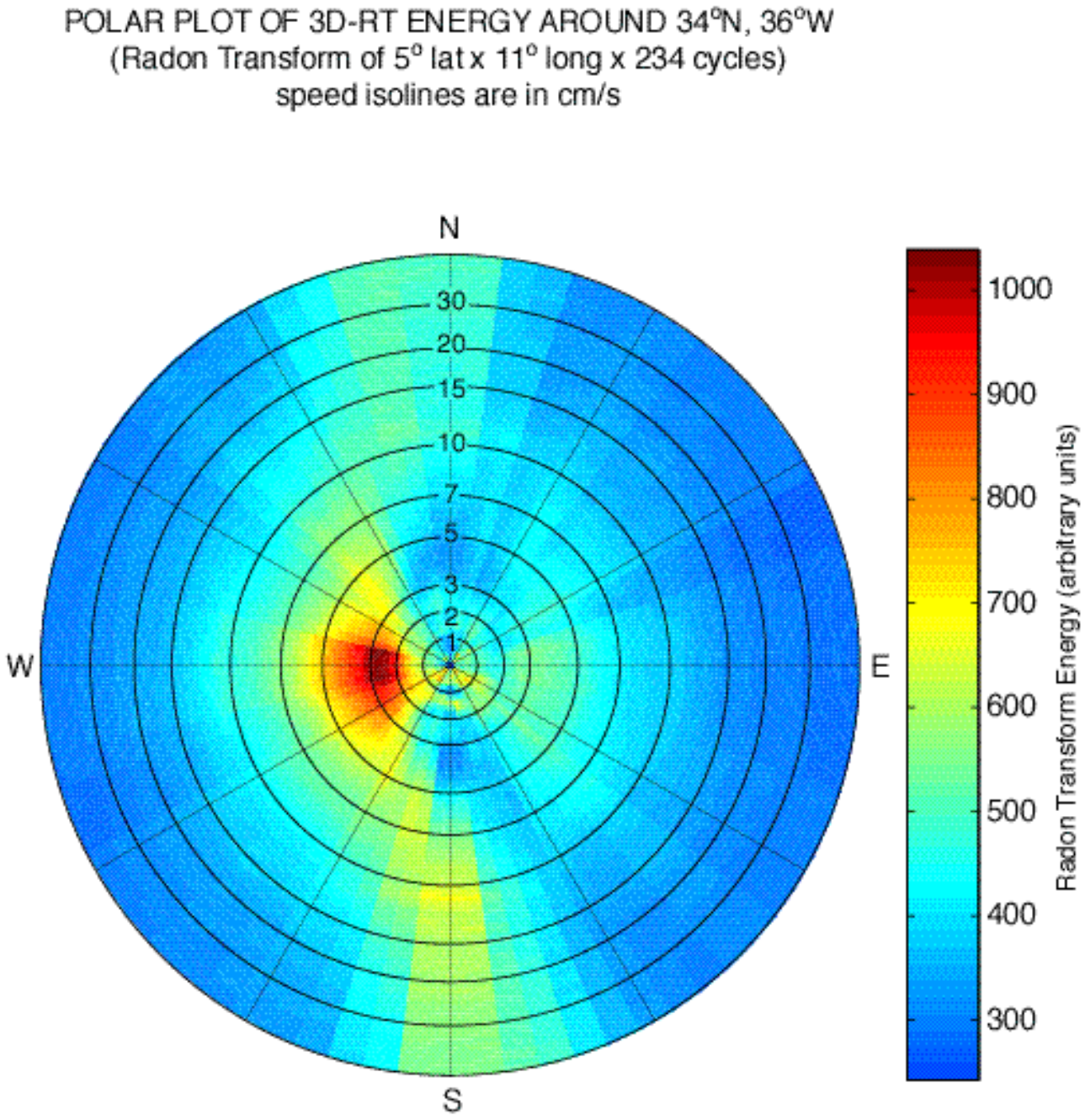
POLAR PLOT OF 3D-RT ENERGY AROUND 34°N, 36°W
(Radon Transform of 5° lat x 11° long x 234 cycles)
speed isolines are in cm/s
N
W
E
S
30
20
15
10
7
5
3
2
1
1000
900
800
700
600
500
400
300
Radon Transform Energy (arbitrary units)

Figure 4.

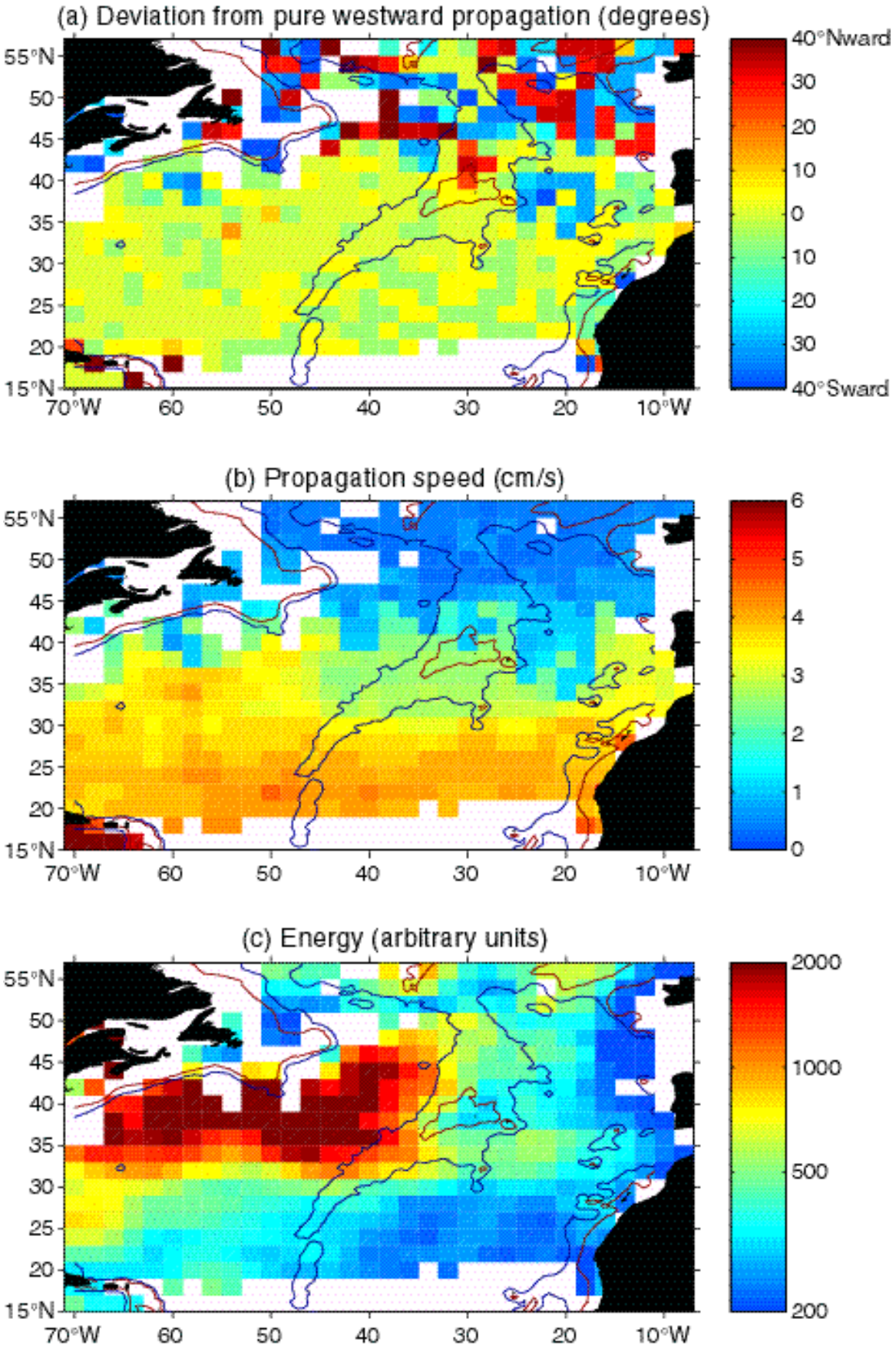
(a) Deviation from pure westward propagation (degrees)
55°N
50
45
40
35
30
25
20
15°N
70°W
60
50
40
30
20
10°W
40°Nward
30
20
10
0
10
20
30
40°Sward
(b) Propagation speed (cm/s)
6
5
4
3
2
1
0
(c) Energy (arbitrary units)
2000
1000
500
200

Figure 5

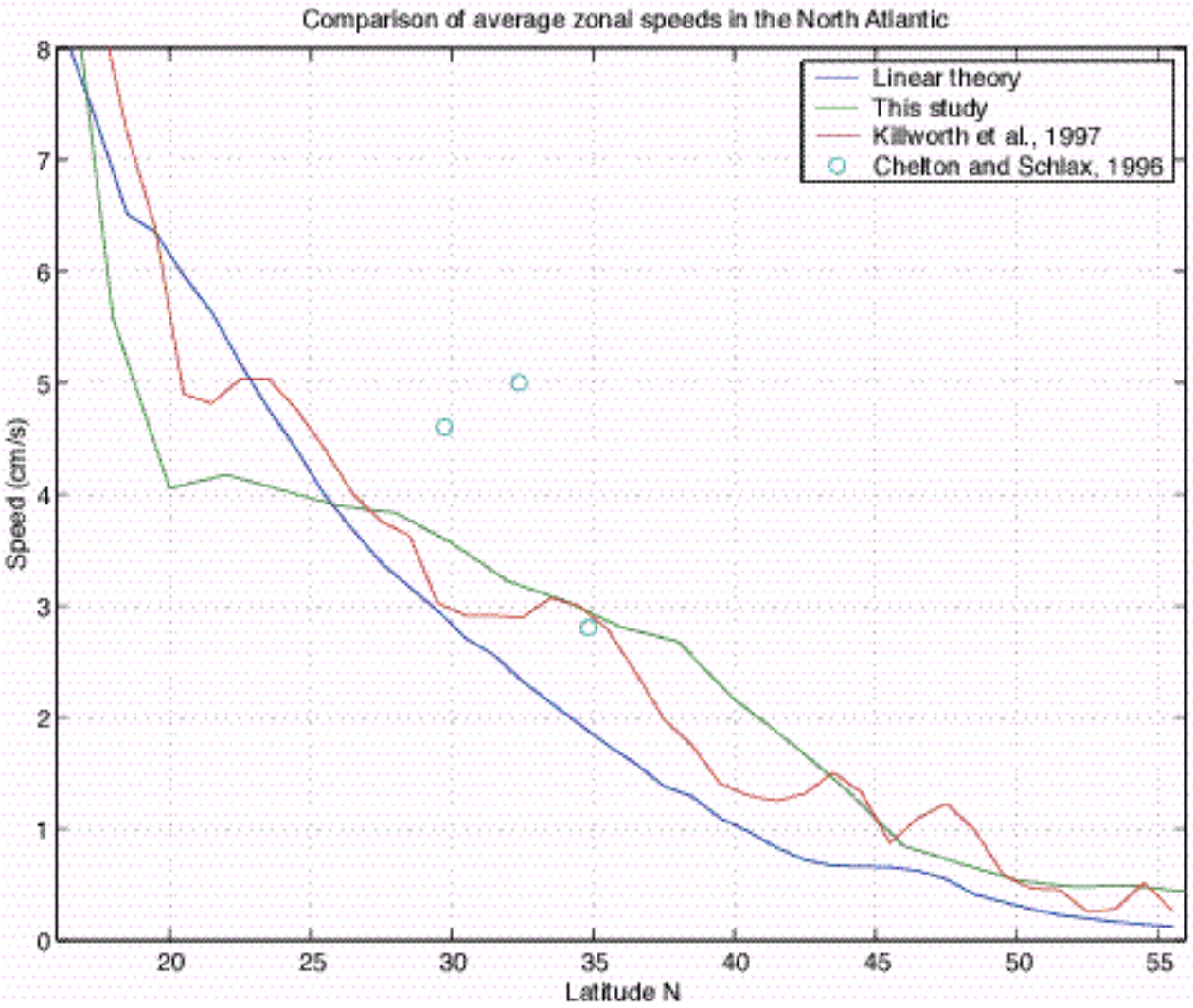
Comparison of average zonal speeds in the North Atlantic
Linear theory
This study
Killworth et al., 1997
Chelton and Schlax, 1996
Speed (cm/s)
Latitude N
0
1
2
3
4
5
6
7
8
20
25
30
35
40
45
50
55

Figure 6